Astron. Astrophys. 326, 1001{1012 (1997)

ASTRONOMY
AND
ASTROPHYSICS

Physics of accretion onto young stars

II. Structure and evolution of accreting stars

Lionel Siess, Manuel Forestini, and Claude Bertout
Observatoire de Grenoble, Laboratoire d'Astrophysique, Universit e Joseph Fourier, B.P.53X, F-38041, Grenoble Cedex, France

Received 10 November 1995 / Accepted 30 May 1997

Abstract. We present new computations of pre-main sequence evolution for stars that accrete a substantial part of their mass. We compute several models with different mass accretion rates, focusing on the effect of deuterium burning on stellar evolution during the accretion phase. We treat accretion not only as a surface boundary condition but as a global phenomenon that affect also the inner parts of the star, using a formalism developed by Siess & Forestini (1996a). We study the effect of varying the mass distribution of accreted matter into the star, and analyze the in uence of different chemical compositions for the accreted matter. We also take into account the possible deposition of accretion energy transported by the accreted matter. We show that accretion can lead to substantial changes in the pre-main sequence evolutionary tracks in the Hertzsprung-Russell diagram (HRD). When accretion stops, the star relaxes to its \standard" track in the HRD, and this, independently of the previous accretion rate.

Key words: accretion { pre-main sequence stars { stellar evolution { Hertzsprung-Russell (HR) diagram

1. Introduction

Over the past few years, much attention has been given to the environment and evolution of young stellar objects. The pres-

influence of chemical composition and the consequences of different mass accretion distributions. In Sect. 4 we compare our results with standard pre-main sequence (PMS) evolution, and in Sect. 5 we examine how accreting stars relax once accretion stops. Finally we summarize and discuss our results in Sect. 6.

2. Numerical procedure

The stellar evolution code used for this study was described in several articles (Forestini 1991,1994), and currently used opacities or atmosphere models are analyzed in detail by Siess et al. (1996b). Modifications needed to take accretion into account are the following.

2.1. Mass and composition update

SF derived the distribution f of accreted matter deposited in the star as a function of its thermal, chemical and mechanical properties. By definition f_j represents the ratio of the mass $\mathrm{d}m_j^a$ accreted in shell j to the mass of this shell, $\mathrm{d}m_j^*$. Therefore, when f is computed, the new mass distribution after accretion, $\mathrm{d}m_j^{*+a}$, is given by[1]

$$\mathrm{d}m_j^{*+a} \;=\; (1+f_j)\,\mathrm{d}m_j^* \;. \tag{1}$$

Our computations reveal that the distribution of matter inside the star does not depend on the mesh point. Indeed in completely convective stars, the accreted matter distributes uniformly in the stellar interior whatever are the distribution of mass shells or time step. On the other hand if the accretion process involves only the surface layers of the star, the periodic redistribution of mass shells has very weak effect because in this region the mass interval between two shells is always very small. Moreover the time step Δt is also constrained by the accretion process and must fulfill $\dot{M}\Delta t < 0.01 M_*$. This condition ensures small changes in function f between two consecutive models.
This modification of the mass distribution is accompanied by a modification of chemical composition, since the chemical composition of the accreted matter is not necessary the same as that of the star. This is especially the case for ^{2}H, as we shall see. Species conservation leads (cf Appendix A) to a new mass fraction of element i at shell j

$$X_{i,j}^{*+a} \;=\; \frac{X_{i,j}^* + f_j\, X_{i,j}^a}{1\,+\,f_j} \;, \tag{2}$$

where $X_{i,j}^*$ is the stellar mass fraction of element i at shell j before accretion and $X_{i,j}^a$ the mass fraction of this element in the accreted matter. In our model we assume that a turbulent element keeps its identity until it dissolves, therefore we can replace $X_{i,j}^a$ by X_i^a in the above expression. As expected, if the chemical composition of the circumstellar environment does not differ from that of the star ($X_{i,j}^* = X_i^a$), there is no chemical change. Additional modifications come from the fact that $X_{i,j}^*$ has to be rescaled to the new mass distribution (Appendix A). The energetic properties of the accreted matter are discussed in the next section.

[1] In the following, superscripts * and ^{a} will refer to variables evaluated in the star before mixing and in the accreted matter, both at time t, while superscript $^{*+a}$ will correspond to the result of mixing.

2.2. Energy equation

During the accretion process, a large amount of potential energy is released. If we assume that accretion is ultimately caused by the presence of an accretion disk around the star, then half of the accretion luminosity is radiated by the disk while the other half L_{bl} is deposited in the boundary layer

$$L_{bl} = \frac{1}{2} L_{acc} = \frac{G M_* \dot{M}}{2\,R_*} \;, \tag{3}$$

where G is the gravitational constant, M_* is the protostellar mass, $\dot{M}$is the mass accretion rate and R_* is the radius of the hydrostatic core. Generally it is assumed that the accreted matter has the same specific entropy as matter on the stellar surface (Kippenhahn et al. 1977, Mercer-Smith et al. 1984, Stringfellow 1989, Braun et al. 1995) but this assumption is not necessarily satisfied. Physical conditions prevailing in the boundary layer are still subject to many uncertainties (Popham et al. 1993, Regev & Bertout 1995). In particular, the fraction of accretion luminosity that is effectively radiated away is still uncertain. We thus use in the following a parameter α ($0 \leq \alpha \leq 1$), representing the fraction of L_{bl} that is transfered to the accreted matter as internal energy, the fraction $(1-\alpha)L_{bl}$ escaping radiatively. The accretion luminosity imparted to the star is written

$$L_{acc,*} = \alpha\, L_{bl} \;. \tag{4}$$

In a situation where $\alpha = 0$, all the energy is radiated away in the boundary layer and the accreted matter mixes with the same properties as the local stellar matter. Conversely, if $\alpha = 1$, L_{bl} is available to heat up the stellar matter.

During an evolutionary time step Δt, a mass $M_{acc} = \dot{M}\Delta t$ is accreted and a total energy $L_{acc,*}\Delta t$ is given to the star. Assuming instantaneous and uniform heat repartition, each gram of accreted matter releases on average, an energy $\varepsilon_{acc} = L_{acc,*}/M_{acc}$ per second. The distribution of ε_{acc} then corresponds to the distribution of accreted matter. In consequence, the value $\varepsilon_{acc,j}$ at shell j is

$$\varepsilon_{acc,j} = \alpha\, \frac{G M_*}{2\,R_* \Delta t}\, \frac{f_j}{1+f_j} \;, \tag{5}$$

where f_j is the accretion function. The factor $(1+f_j)^{-1}$ takes into account the mass modification of the shells. This relation satisfies $\int \varepsilon_{acc}\, \mathrm{d}m^{*+a} = L_{acc,*}$.
The fact that accreted matter can radiate and lose part of its heat excess during the accretion process is explicitly taken into account by the function f. Actually, the distribution of mass deposition inside the star depends on the thermal property of the accreted material (see the discussion in SF).

Finally, the equation of energy conservation can be written

$$\frac{\partial L_r}{\partial m} \;=\; \varepsilon_{nuc} + \varepsilon_{grav} + \varepsilon_{acc} \;,$$

where L_r is the local luminosity and where ε_{nuc} (ε_{grav}) is the nuclear (gravitational) energy production rate per unit mass.

2.3. Nucleosynthesis and accretion

During classical PMS evolution, the luminosity L_* is provided by the gravitational contraction and the star evolves on the Kelvin-Helmholtz time scale, τ_{KH} defined by

$$\tau_{KH} \sim \frac{GM_*^2}{2R_*L_*} .$$

For a star of $1\,M_\odot$, τ_{KH} is of the order of 10^7 yr. Deuterium ignition in the early evolution does not alter the general evolution; it only slows the stellar contraction. This is due to both the small amount of deuterium (the deuterium mass fraction is $X_D = 4.67\,10^{-5}$) and its very high burning rate, which do not maintain nuclear energy production during more than $\sim 10^5$ yr.

However, inclusion of the accretion process modifies that scheme. As long as matter is accreted (typically a few million years), the nuclear energy production is maintained by the inflow of fresh deuterium. The deuterium production due to the nuclear reactions

$$^9\mathrm{Be} + \mathrm{p} \rightarrow {}^2\mathrm{H} + 2\,{}^4\mathrm{He}$$
$$^1\mathrm{H} + {}^1\mathrm{H} \rightarrow {}^2\mathrm{H} + \nu_e + \mathrm{e}^+$$

is negligible compared to the inflow of fresh deuterium. From now on, the structure is governed by nuclear burning and evolves on a nuclear time scale. In order to decouple the equations of nucleosynthesis from those of stellar structure we normally have to constrain the time step to be small enough to guarantee a constant deuterium abundance over the time step. I.e., the evolutionary time step reduces to a few hundred years. In other words, the evolution of deuterium abundance in the presence of accretion cannot be treated independently from the overall evolution of stellar structure.

During a time step Δt, accreted material brings in the star a number of deuterium atoms $n_D^a = (X_D^a \dot{M} \Delta t)/m_D$, where X_D^a is the deuterium mass fraction in the accreted matter and m_D the mass of the deuterium atom. The equation governing deuterium abundance evolution is then given by[2]

$$\frac{\mathrm{d}n_D^{*+a}}{\mathrm{d}t} = -\frac{n_D^*}{\tau_{dest}} + \frac{X_D^a \dot{M}_{acc}}{m_D} = -\frac{n_D^*}{\tau_{dest}} + \frac{n_D^a}{\Delta t} , \quad (6)$$

where τ_{dest} is the characteristic time scale of deuterium burning, n_D^* and n_D^{*+a} the number density of deuterium in the star before and after addition of accreted matter. Usually the nucleosynthesis equations are written in terms of the mole fraction Y_D, a quantity that is related to n_D by

$$n_D = \mathcal{N}_{av}\rho\frac{X_D}{A_D} = \mathcal{N}_{av}\rho Y_D , \quad (7)$$

where $\mathcal{N}_{av}$ is the Avogadro number, ρ the density and A_D the deuterium mass number. From Eq. (7), we have

$$\frac{\mathrm{d}n_D}{\mathrm{d}t} = \mathcal{N}_{av}\Big(Y_D\frac{\mathrm{d}\rho}{\mathrm{d}t} + \rho\frac{\mathrm{d}Y_D}{\mathrm{d}t}\Big) . \quad (8)$$

[2] From now on, the shell subscript j will be omitted.

This expression couples the structural and nucleosynthetic evolution. The evolutionary time-step we choose for each model must verify the following equation in each shell of the star

$$\frac{\Delta\rho}{\rho} = \frac{\mathrm{d}\rho}{\mathrm{d}t}\frac{\Delta t}{\rho} < 10\% , \quad (9)$$

where $\Delta\rho$ is the density difference between the two last successfully calculated models. Condition (9) allows us to neglect density time-variations in Eq. (8), so that Eq. (6) simplifies to

$$\rho^{*+a}\frac{\mathrm{d}Y_D^{*+a}}{\mathrm{d}t} = -\rho^*\frac{Y_D^*}{\tau_{dest}} + \rho^a\frac{Y_D^a}{\Delta t} , \quad (10)$$

where Y_D^a is the mole fraction of deuterium in the accreted matter. Mass accretion causes a dilution of the shells and to account for that, we define new variables, $\widetilde{Y}_D^*$ and $\widetilde{Y}_D^a$ as

$$\widetilde{Y}_D^* \equiv \frac{\rho^*}{\rho^{*+a}}Y_D^* \equiv \frac{1}{1+f}Y_D^* \quad (11)$$

$$\widetilde{Y}_D^a \equiv \frac{\rho^a}{\rho^{*+a}}Y_D^a \equiv \frac{f}{1+f}Y_D^a . \quad (12)$$

Finally the general equation governing the evolution of deuterium is

$$\frac{\mathrm{d}Y_D^{*+a}}{\mathrm{d}t} = -\frac{\widetilde{Y}_D^*}{\tau_{dest}} + \frac{\widetilde{Y}_D^a}{\Delta t} , \quad (13)$$

the formal solution of which is given by

$$Y_D^{*+a} = \widetilde{Y}_D^*\,\exp(\frac{-\Delta t}{\tau_{dest}}) + \widetilde{Y}_D^a\frac{\tau_{dest}}{\Delta t}\big(1-\exp(\frac{-\Delta t}{\tau_{dest}})\big) . \quad (14)$$

The first term in Eq. (14) gives the deuterium abundance after its nuclear depletion during a period Δt. The second term represents the contribution due to accretion including the partial destruction of this element during Δt. In the very early evolution, the reaction rate is very slow ($\tau_{dest} \rightarrow \infty$) and we find that

$$Y_D^{*+a} = \widetilde{Y}_D^* + \widetilde{Y}_D^a = Y_D^a = Y_D^* ,$$

i.e. the composition remains unchanged. This equation is solved, during the convergence process, at each iteration for the stellar structure.

2.4. Treatment of convective regions

In convective regions, we assume instantaneous mixing. The chemical elements are homogenized and the resulting mean abundances are given by

$$\overline{X_i} = \frac{\int_{M_b}^{M_t} X_i(m)\,\mathrm{d}m}{(M_t - M_b)} , \quad (15)$$

where X_i is the mass fraction of element i, M_b and M_t the mass coordinates of the bottom and the top of the convective zone, respectively. Applied to Eqs. (11) and (12) this leads to

$$\overline{\widetilde{Y}_D^a} = \Big(\frac{M^a}{M^{*+a}}\Big)_{cz} Y_D^a \quad (16)$$

and

$$\overline{\widetilde{Y}_D^{*}} = \left(\frac{M^*}{M^{*+a}}\right)_{cz} Y_D^* \,, \tag{17}$$

where M_{cz}^* is the mass of the convective region, M_{cz}^a the mass accreted in this zone and $M_{cz}^{*+a} = M_{cz}^* + M_{cz}^a$.

Furthermore, as we make the assumption of completely homogeneous convective regions, nucleosynthesis within this zone can also be calculated in one shot, in a mean fictitious shell where we consider the average destruction time scale

$$\bar{\tau}_{dest}^{-1} = \frac{\int_{M_b}^{M_t} \tau_{dest}^{-1}(m)\,\mathrm{d}m}{(M_t - M_b)} \,. \tag{18}$$

The average is made on τ_{dest}^{-1} because it represents the mean reaction rate. Thus, inside convective regions, deuterium evolves according to

$$\begin{aligned} Y_D(t+\Delta t) \;=\; & \overline{\widetilde{Y}_D^{*}}(t)\,\exp\!\left(\frac{-\Delta t}{\bar{\tau}_{dest}}\right) \\ & +\; \overline{\widetilde{Y}_D^{a}}\,\frac{\bar{\tau}_{dest}}{\Delta t}\left(1 - \exp\!\left(\frac{-\Delta t}{\bar{\tau}_{dest}}\right)\right) . \end{aligned} \tag{19}$$

3. Results and discussion

3.1. Initial model and accretion rates

Our initial models result from a polytropic model with index n=1.5. After convergence with our evolution code, we obtain a 0.5 $\mathrm{M}_\odot$ star, with a radius $R \sim 5\,R_\odot$, a luminosity $L \sim 6.5 L_\odot$, an effective temperature $T_{\rm eff} \sim 4000$ K and a central temperature $T_c \sim 7 \times 10^5$K. It is completely convective, surrounded by a thin radiative atmosphere. It is also located above the birthline defined by Stahler (1988). In the future, a more consistent approach would be to combine both the protostellar (spherical) and PMS (axisymetric) accretion phases. For self-consistent computations, these two consecutive phases will require the same constitutive physics.

Concerning the accretion model, default parameters are ξ = 0.01, Ri^- = −10, $\mathcal{E}^a$ = 0.8 and α = 0.01. We remind the readers that ξ represents the fraction of the Keplerian angular momentum at the stellar surface that is injected into the star, Ri^- the value of the Richardson number in the convective region and $\mathcal{E}^a$ characterizes the thermal behavior of the accreted matter. As explained in SF, a large negative value of Ri^- depicts a situation close to free convection where the mass distribution remains unchanged. If the accreted globule rapidly thermalizes, i.e., if $\mathcal{E}^a \ll 1$, the accretion process does not disturb the convective motions and matter distributes uniformly. In the following, we will show the influence of changing these parameters. The chemical composition of the accreted matter is assumed identical to the initial composition of the star. Initial abundances are X = 0.6867, Y = 0.2932 and Z = 0.02.

In order to illustrate the effects of accretion on stellar evolution, we study three time variable accretion rates typical of extreme T Tauri stars (Adams et al. 1990) and limit the computations to a maximum mass of 1.2 $\mathrm{M}_\odot$. The time accretion

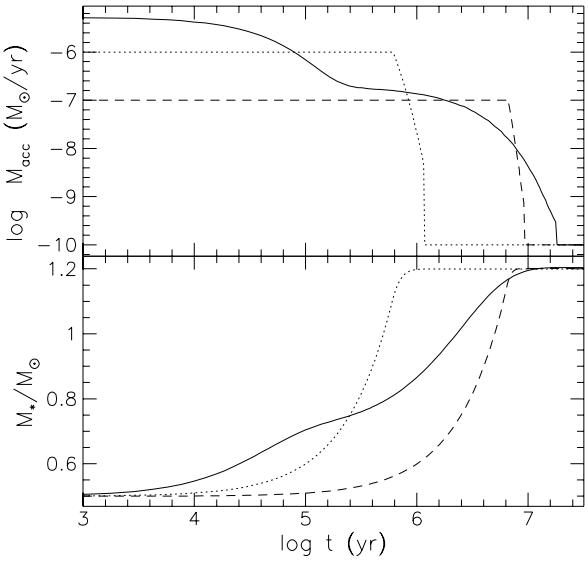

Fig. 1. Accretion rates (above) and mass evolution (below). The accretion end corresponds a final mass of 1.2 $M_\odot$. The solid line refers to the exponential law (R3), while the dotted and dashed curves correspond to the (R1) and (R2) prescriptions, respectively.

laws, in the unit of $\mathrm{M}_\odot\ \mathrm{yr}^{-1}$, are given by

$$\begin{aligned} &10^{-6} \;\; \text{if} \;\; \mathrm{M} < 1.10\,\mathrm{M}_\odot \;\; \text{else} \;\; 10^{-6}\exp -t/\tau_1 && \text{(R1)} \\ &10^{-7} \;\; \text{if} \;\; \mathrm{M} < 1.15\,\mathrm{M}_\odot \;\; \text{else} \;\; 10^{-7}\exp -t/\tau_2 && \text{(R2)} \\ &5\times10^{-6}\exp -t/\tau_3 + 2\times10^{-7}\exp -t/\tau_4 && \text{(R3)} \end{aligned}$$

with τ_1, τ_2, τ_3, τ_4 equal to 10^5, 5×10^5, 4×10^5 and 2.5×10^6 yr, respectively. These functions are depicted in Fig. 1. The accretion law (R3) accounts for a large accretion phase at the beginning of the evolution followed by a slowly decreasing accretion activity. We first study the accretion phase, i.e., ages lower than 10^7yr.

3.2. Energetic evolution of accreting stars

At the beginning of their evolution, stars are completely convective and lie on the Hayashi portion of their PMS track. Their internal pressure cannot balance gravity and they contract. When the central temperature reaches 10^6 K, deuterium ignites through the reaction

$$^1\mathrm{H} + {}^2\mathrm{H} \rightarrow {}^3\mathrm{He} + \gamma \,. \tag{20}$$

This event marks the beginning of a different evolutionary phase for accreting stars.

For completely convective stars, the central temperature can be approximated by

$$T_c \approx 1.2 \times 10^7\,\mu\,\frac{M_*}{M_\odot}\,\frac{R_\odot}{R_*}\ \mathrm{K} \,, \tag{21}$$

where μ is the mean molecular weight (Cox & Giuli, 1968). Eq. (21) indicates that the rate of increase of T_c depends on the contraction and mass accretion rates. Prior to deuterium

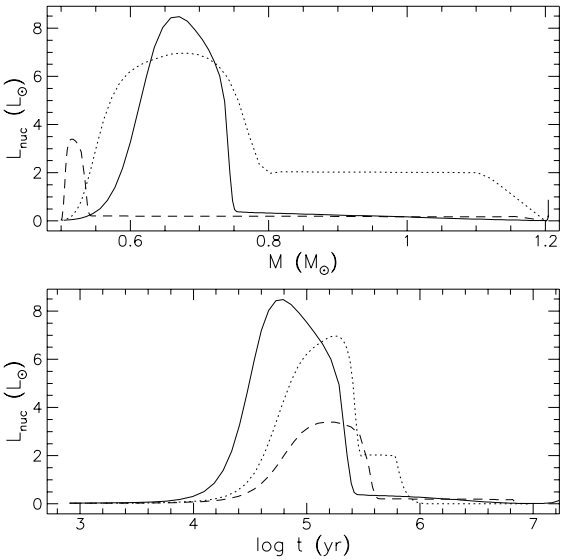

Fig. 2. The nuclear luminosity L_{nuc} of our accreting stars for the three accretion rates as a function of their increasing total mass (upper panel) and as a function of time (lower panel). Default parameters are $\xi = 0.01$, $Ri^{-} = -10$, $\mathcal{E}^a = 0.8$ and $\alpha = 0.01$. Curves are plotted with the same conventions as Fig. 1.

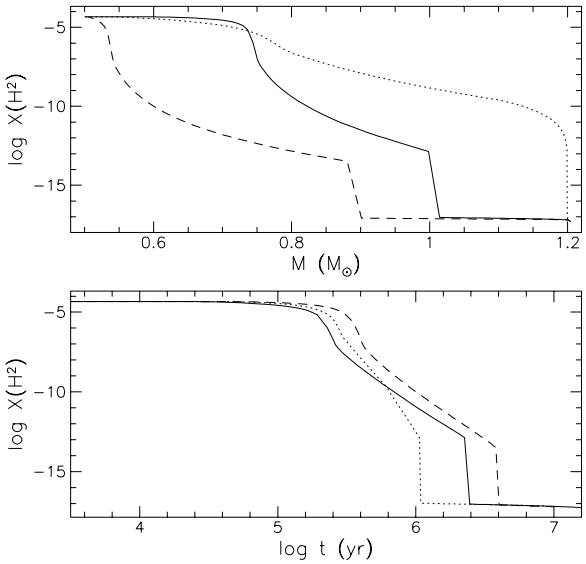

Fig. 3. Central deuterium mass fraction as a function of mass (upper panel) and as a function of time (lower panel) for the different accretion rates. Curves are plotted with the same conventions as Fig. 1.

ignition, the radius evolution is not very sensitive to $\dot{M}$(Fig. 4) so deuterium first ignites inside the more massive stars, i.e., those accreting at the largest rates (Fig. 2). When nuclear energy production begins, the amount of deuterium is larger in more massive stars and the generated luminosity more important. Changes of initial conditions will not affect this result. Indeed the more distended is the star in its initial configuration, the faster it contracts and by the time deuterium ignites, a very short time elapses (typically a few thousand years). Therefore, the temperature of deuterium ignition is reached with a mass close to its initial value, almost independent of the initial conditions.

Once X_D decreases significantly due to the increasing central temperature, the luminosity drops, reaching its equilibrium value defined by

$$L_{eq} \;=\; \mathcal{N}_{av} Y_D^a \, Q_D \, \dot{M} \,, \tag{22}$$

where Q_D is the energy generated per reaction (Q_D = 5.5 Mev) and Y_D^a the constant mole mass fraction in the accretion disk. For illustration, we show in Fig. 3 the deuterium mass fraction as a function of time. When L_{nuc} reaches its maximum, most of the deuterium initially present in the star has been burned. The increasing reaction rate contributes to deplete deuterium abundance which now settles to an equilibrium value X_{eq}, defined by

$$X_{eq} \;=\; A_D \widetilde{Y}_D^a \frac{\tau_{dest}}{\Delta t} \,. \tag{23}$$

X_{eq} represents the solution of Eq. (14) in the limit of very fast reaction rate ($\tau_{dest} \rightarrow 0$). The further drop of ^{2}H seen in Fig. 3 is due to either the end of accretion for the dotted line (R1), or to the appearance of a radiative core that prevents deuterium from reaching the center for (R2, R3). We see that high accretion rates can sustain a high deuterium abundance despite the increasing reaction rate. The tremendous energy generated by deuterium burning during the accretion process is reflected in the stellar structure.

3.3. Internal structure

The nuclear luminosity due to deuterium burning during the accretion phase, is so strong that it exceeds the stellar luminosity. The overall stellar gravitational energy becomes negative (Fig. 4) and the star undergoes a global swelling. In the non-accreting case or for low accretion rates[3], this phenomenon is not present because deuterium is exhausted too rapidly to cause an increase in L_{nuc}. Expansion lasts as long as $L_{nuc} > L_*$, i.e., as long as the star has not reached thermal equilibrium. For large accretion rates ($\dot{M} > \dot{M}_c$) or early in the evolution when the accretion time scale $\tau_{acc} \sim M_*/\dot{M}$ is smaller than the Kelvin-Helmholtz time scale, the nuclear energy production induced by the accretion process dominates the structural evolution and the star expands. When sufficient mass has been accreted, the increased gravitational potential finally limits the swelling.

The dilatation of the star provokes a drop of central density and halts temporarily the central temperature increase as indicated in Fig. 5a–d. The large energy production at the onset of deuterium burning warms up the central regions but the great sensitivity of the reaction rate on temperature (Caugh-

[3] Neglecting deuterium burning, Hartmann & Kenyon (1990) determined a critical accretion rate $\dot{M}_c$ above which the contraction of the PMS star can be halted ($\dot{R} = 0$). They found $\dot{M}_c \sim \dfrac{7RL}{6GM^2}$, which corresponds to $\dot{M}_c \sim 10^{-6} \mathrm{M}_\odot \ \mathrm{yr}^{-1}$.

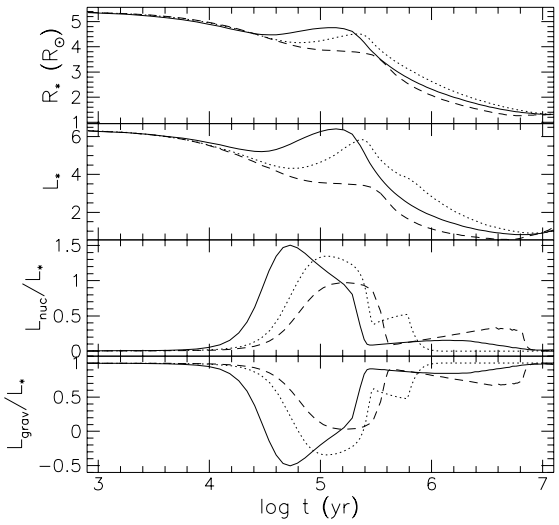

Fig. 4. Influence of the accretion rate on the stellar radius and luminosities. From the top to bottom panels, are depicted the stellar radius, the total, nuclear and gravitational luminosities, respectively. Curves are plotted with the same conventions as Fig. 1.

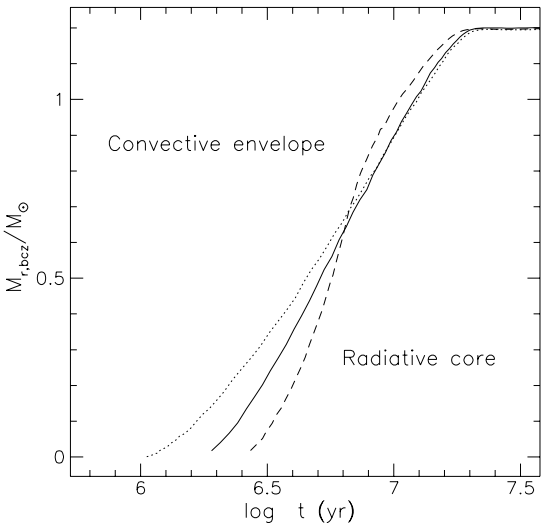

Fig. 6. Mass at the base of the convective envelope. This graph shows the development of the radiative core for the different accretion rates. Initially the star is completely convective and due to the drop in opacity the radiative core suddenly appears. Curves are plotted with the same conventions as Fig. 1.

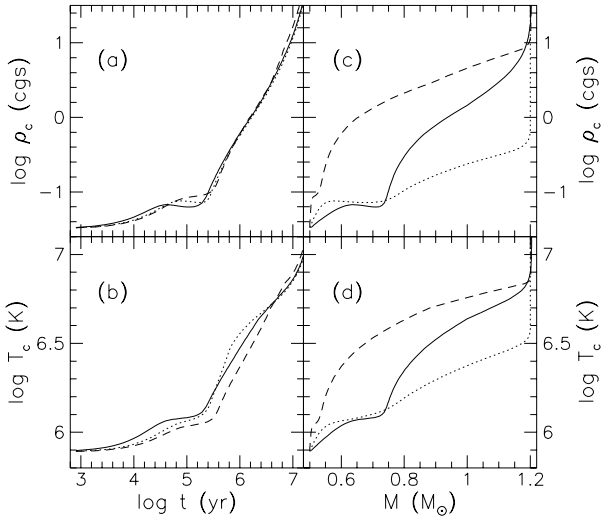

Fig. 5a–d. Central density and temperature as a function of time [**a** and **b**] and as a function of mass [**c** and **d**] for the different accretion rates. We note the thermostatic effect of deuterium burning that maintains T_c to an almost constant value as long as $L_{nuc} > L_*$. Curves are plotted with the same conventions as Fig. 1.

lan & Fowler 1988) forces deuterium to burn thermostatically, preventing the temperature from climbing too much. This is particularly marked in Fig. 5a–d.d for high accretion rates. However when a significant fraction of the deuterium is depleted, the nuclear energy production can only be maintained by an increase of the central temperature. At that time, the star is still completely convective and its gradient ∇ is nearly adiabatic, so that $P \sim T^{5/2}$. For an ideal gas with a constant mean molecular weight μ (true even during deuterium burning because of the relatively low ^{2}H abundance level), one obtains $\rho \sim T^{3/2}$. Therefore temperature variations modify in the same way the other thermodynamic quantities P_c and ρ_c.

Another interesting property of these models is the influence of accretion on the formation of the radiative core. In Fig. 6, we see that the formation of the radiative core depends on the accretion scenario. During PMS evolution, the opacity κ continuously drops in the deep interior with rising central temperatures until the radiative temperature gradient becomes smaller than the adiabatic gradient. However, the maintenance of an important nuclear energy production at the star's center forces the radiative gradient to remain larger than the adiabatic one, so that the star remains convectively unstable. Finally, with decreasing accretion rate and nuclear burning rate, the star turns radiative in its center. The radiative core grows rapidly in mass and forms a radiative barrier that stops the freshly accreted matter. The rate of core growth depends on the central temperature at the time of its formation.

3.4. Influence of the chemical composition

We present here the effect of varying the deuterium abundance since it may vary from different regions of the interstellar medium. The evolutionary influence of deuterium can be gauged by artificially varying its interstellar concentration. For the purpose of the study, we have computed for a constant accretion rate given by relation (R1), three different evolutionary models where deuterium mass fraction was set to X_D = 4.65 $\times$ 10^{-4} and 4.65 $\times$ 10^{-6} instead of 4.65 $\times$ 10^{-5}.

We notice from Fig. 7 that a lower abundance reduces the nuclear luminosity and postpones deuterium ignition. Indeed,

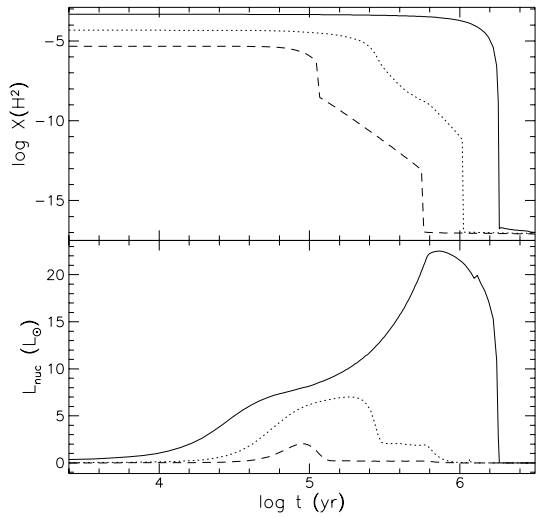

Fig. 7. Effect of deuterium abundance on the generated nuclear luminosity. For an accretion prescription given by relation (R1), the evolution of the abundance and the nuclear luminosity are plotted as a function of time. The dotted lines refers to the interstellar value of $X_{D,ISM}$, the solid and dashed curves to X_D equal $10 \times X_{D,ISM}$ and $X_{D,ISM}/10$, respectively.

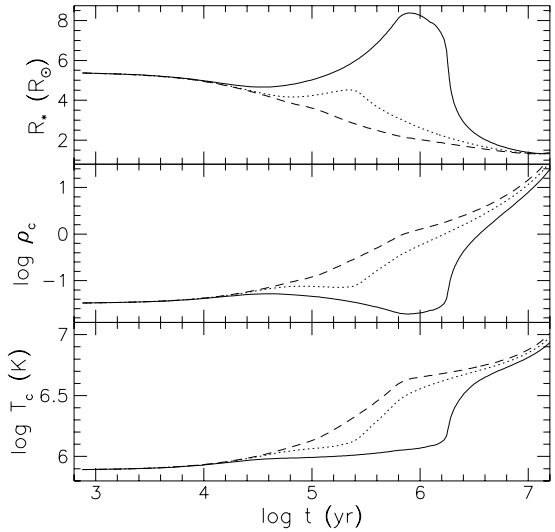

Fig. 8. Influence of deuterium abundance on the radius, central density and temperature. Curves are plotted with the same conventions as Fig. 7.

the rate of nuclear energy production per unit mass ε_{nuc}, can be written in the form

$$\varepsilon_{nuc} = \mathcal{N}_{av} \frac{Y_D^* Q_D}{\tau_{dest}} . \quad (24)$$

Therefore, a higher deuterium mass fraction is able to produce a larger ε_{nuc} at a given time than in a standard case.

The flat deuterium mass fraction profile observed for the largest initial abundances is due to the great temperature sensibility of reaction (20); the star reacts to the increased mass

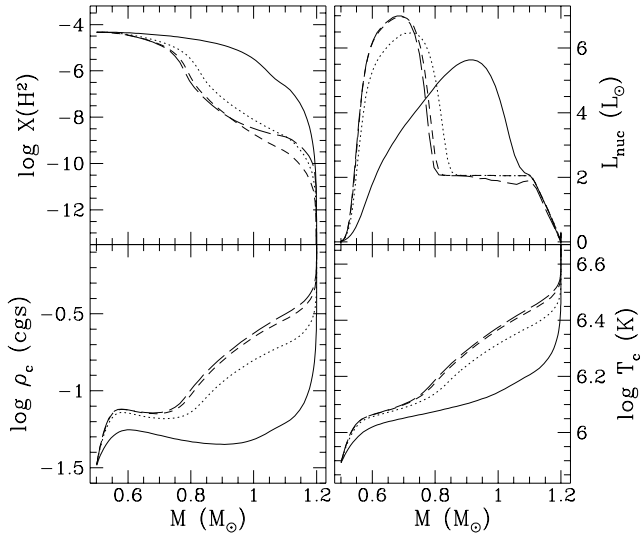

Fig. 9. Influence of accretion energy deposition on the central temperature and density, on the deuterium mass fraction and nuclear luminosity. The solid, dotted, short- and long-dashed lines correspond to a value of α equal to 0.5, 0.1, 0.01 and 0, respectively. The accretion rate is $\dot{M} = 10^{-6}$ M$_\odot$ yr^{-1}, $Ri^- = -10^3$, $\mathcal{E}^a = 0.9$ and $\xi = 0.01$.

fraction and generated luminosity by burning deuterium at a slower rate and thus for a longer time. The mechanical consequence is a substantial swelling of the entire star, an effect not present for low abundances (Fig. 8).

Although a deuterium abundance ten times greater than its interstellar value would provide the same equilibrium luminosity than an accretion rate ten times larger [Eq. (22)], the behavior of the star is completely different. During all the accretion process, it is a combination of both $\dot{M}$and X_D that governs the evolution of the structure, and depending on these values the star can experience either a swelling or a contraction.

3.5. Effect of accretion energy deposition

We study the role of accretion energy deposition in the star. The control parameter α, defined in Sect. 2.2, allows us to treat accretion not only as a mechanical constraint to the structure, but also as an energetic process.

Faced with the arrival of accretion energy, the star converts the thermal energy of accreted matter principally into work against compression rather than into internal energy and consequently expands. This results from the thermostatic effect of deuterium burning which constraints temperature to weak variations. Fig. 9 displays the effect of this additional source term on the central density and temperature. When a large amount of accretion energy is released, the temperature enhancement is less pronounced and consequently deuterium is depleted more slowly (Fig. 9). The difference in the deuterium profile for $\alpha = 0.01$ and $\alpha = 0$ (short- and long-dashed lines, respectively) reflects the temperature sensitivity of the reaction rate.

The larger ε_{acc}, the later deuterium is depleted and, in extreme cases where most of the accretion luminosity is driven

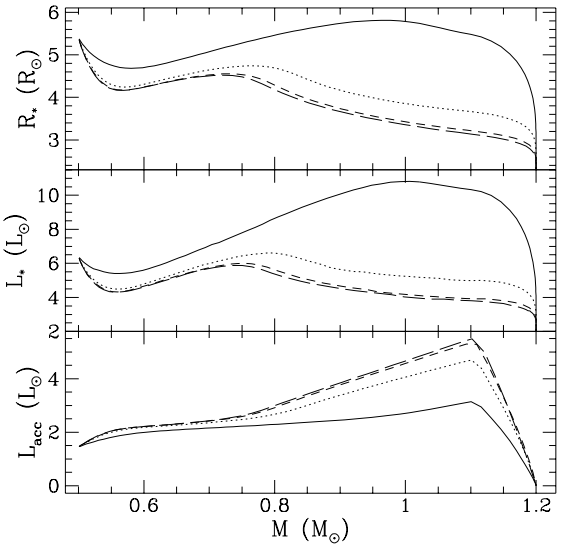

Fig. 10. Influence of accretion energy deposition on the radius (top panel), the stellar (mid panel) and accretion luminosity (lower panel). Curves are plotted with the same conventions as Fig. 9.

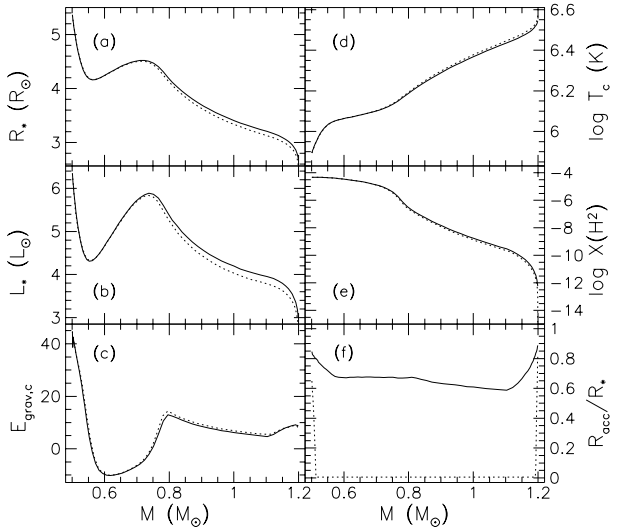

Fig. 11a–f. Comparative study of relevant variables for two different distributions of accreted matter. The solid line refers to a model with $Ri^- = -10$ while the dotted line corresponds to $Ri^- = -10^3$. $\mathcal{E}^a$, ξ and α are fixed to 0.5, 0.01 and 0, respectively, and the accretion law is given by the (R1) prescription. From the top to the bottom and from the left to the right, panels depict respectively the evolution of the stellar radius R_*, stellar luminosity L_*, gravitational energy at the center E_{grav}, central temperature T_c, central deuterium abundance X(^{2}H), and at the right bottom the depth of accretion R_{acc}. R_{acc} equal zero means that accreted matter reaches the center of the star.

into the star (α close to unity), the burning rate is so slow that deuterium abundance remains constant for a longer period, up to one third of the total age of a star. The resulting swelling of the star lowers the inflow of accretion energy ($L_{bl} \propto R^{-1}$) and decreases the thermal relaxation time scale ($\tau_{KH} \propto (RL)^{-1}$). Consequently radius and luminosity will become larger for greater α (Fig. 10). Once accretion ends, the star is already in thermal equilibrium and contraction proceeds.

3.6. Influence of mass accretion profile

To see how changes in various parameters (Ri^-, ξ, $\mathcal{E}^a$) modify the stellar structure, we will first analyze two models with the same accretion law (R1), $\xi = 0.01$ and $\mathcal{E}^a = 0.5$ but with two different values for Ri^-, namely $Ri^- = -10^3$ and $Ri^- = -10$. For $Ri^- = -10^3$, convection transport is efficient and accreted matter reaches the central regions while for $Ri^- = -10$, it mainly accumulates in the outer layers of the star (Fig. 11a–f.f). For both values of Ri^-, we study two models one with and one without accretion energy supply ($\alpha = 0.3$ and $\alpha = 0$).

In the absence of accretion energy inflow ($\alpha = 0$), changes in the parameters have little influence on the evolution of the star because nuclear energy production is not modified. Indeed, for completely convective stars, Eqs. (16,17,19) are independent on the distribution of accreted material. Therefore, if the same amount of matter is accreted, neither Y_D nor the ε_{nuc} profiles given by Eq. (24) will differ in both configurations. Consequently, changes of parameters will not change the role played by deuterium burning and the stellar structure will be almost insensitive to the accreted mass distribution.

As matter penetrates deeper the gravitational potential is reinforced in the central regions and locally the star undergoes a more efficient contraction (Figs. 11a–f). The sharp growth of ε_{grav} at the surface results from the rise of f in the photospheric layers and to the boundary conditions. The star is now somewhat more compact and its higher gravity provides a larger central temperature leading to earlier deuterium depletion. As the effective temperature is almost constant, the luminosity and outer radius decrease.

When mass deposition is accompanied by energy deposition ($\alpha \neq 0$), temperature and nuclear energy rate distributions are modified. If accretion energy is preferentially deposited in the central region ($|Ri^-| \gg 1$), conversion of ε_{acc} into work against compression must be more efficient to prevent a temperature enhancement. Consequently the star has lower average gravitational pull and its radius and luminosity increase (Fig. 12a–f). Conversely, if $L_{acc,*}$ is concentrated in the outer layers of the star, a significant fraction of the accretion energy can be radiated from the surface. As a consequence, the specific entropy is lower and the star contracts more efficiently, yielding a higher central temperature and smaller luminosity.

3.7. Hertzsprung-Russell diagram

The evolution of accreting stars in the HRD is given in Fig. 13. Symbols indicate the most interesting events occurring in these accreting stars. At the beginning of its evolution, an accreting star is located on the Hayashi track corresponding to its initial mass. Contraction proceeds until the central temperature reaches roughly 10^6K, i.e., when deuterium ignites. Within a few thousand years, the nuclear luminosity becomes higher than the surface luminosity (triangle) and forces the star to swell.

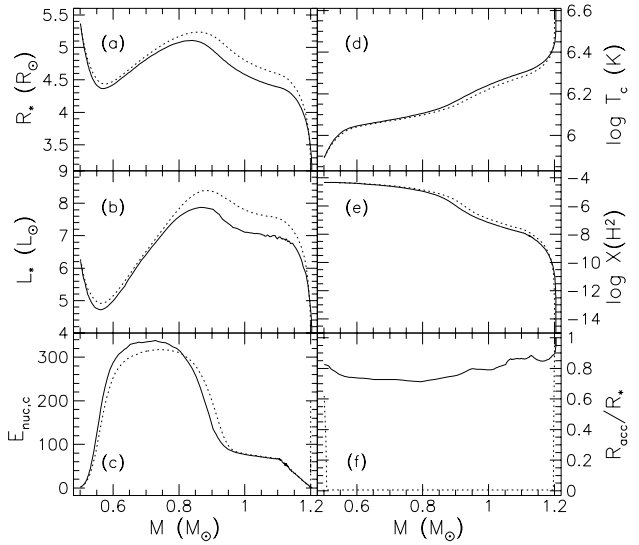

Fig. 12a–f. Same curve as Fig. 11a–f, but for α = 0.3

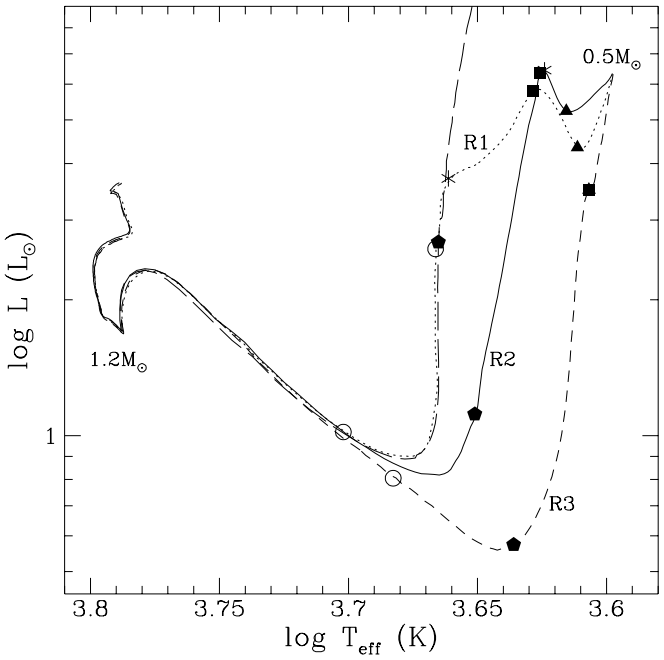

Fig. 13. The evolutionary tracks in the HRD of Z = 0.02 accreting stars. The solid, dotted and short-dashed curves correspond to three different accretion rates: bi-exponential (R3), constant at 10^{-6}M$_\odot$ yr^{-1}(R1) and constant at 10^{-7}M$_\odot$ yr^{-1}(R2), respectively. In our scenario, the end of the accretion phase for the (R1) and (R2) prescriptions is modeled by an exponential decrease. The initial mass is 0.5 M$_\odot$ and the accretion is stopped when the stellar mass reaches 1.2 M$_\odot$. The long-dashed line represents the standard PMS track of a 1.2$M_\odot$ star. Triangles mark the beginning of the star expansion due to deuterium ignition and squares the return to contraction. The radiative core appears in the pentagon location and the open circles mark the end of accretion. In the case of small accretion rate (R2 prescription), triangles and squares are merged and represent the minimum in gravitational luminosity. Stars indicate the time from which the accretion rate falls below 5×10^{-7} M$_\odot$ yr^{-1}.

However depletion of initial deuterium causes a drop in the nuclear energy production; the star undergoes contraction again (square). The next important step in the evolution of the structure is the appearance of the radiative core (pentagon). Finally accretion ends (open circle) and the star relaxes to the standard track corresponding to final mass 1.2 M$_\odot$.

Comparing tracks corresponding to various accretion rates, some general conclusions emerge: (i) the motion of accreting stars in the HRD is always directed to higher effective temperature[4], (ii) the locus of these stars in the HRD is bounded by the two standard PMS tracks corresponding to their initial and final mass and (iii) all accreting stars converge to the same standard track defined by their final mass.

We emphasize on the fact that the luminosity given in Fig. 13 represents the photospheric luminosity only. We do not consider here the circumstellar environment of these objects nor the large amount of energy released by the disk or through the boundary layer. The total luminosity L_{tot} seen by an observer is in fact the composition of the different sources

$$L_{tot} = L_* + (1 - \alpha)L_{bl} + L_{disk} \ ,$$

where L_{disk} is the luminosity emanating from the disk. All these components could also potentially modify the effective temperature and luminosity of the global system, star plus circumstellar surrounding (Kenyon & Hartmann 1990). A confrontation with observations will be presented in Siess et al. (1997).

4. Comparison with standard PMS evolution

We now compare the main properties of accreting PMS stars to those derived from classical pre-main sequence evolution (Siess et al. 1996b). We note that effective temperatures are very similar in both cases, a general feature that results from the fully convective status of these young low mass stars. The nuclear energy production due to deuterium burning heats up the central part of the star and provides higher central temperature and smaller outer radius [Eq. (21)]. The effective temperature being confined in a narrow range, luminosity ($L \propto R^2$) is lower than in the standard scheme.

Comparing the apparent ages of accreting and non accreting PMS stars is a non-trivial matter.
Consider the position in the HRD where the evolutionary track of an accreting star crosses the standard PMS track of a star of given mass. Both stars have thus the same effective temperature $T_{\rm eff}$ and luminosity L and so the same outer radius R, i.e.[5],

$$R^a(t^a) = R^s(t^s) \ , \qquad (25)$$

[4] The evolving star remains located on the Hayashi line corresponding to its instantaneous mass, and cannot therefore move to the right in the HRD (Hayashi 1961)

[5] In the following, superscripts s and a will refer to the standard and accreting stars, respectively.

Table 1. Ages estimation from the position in the HRD when the different accreting stars (R1, R2 and R3) reach $M_* = 0.9\,M_\odot$ and when they first reach their standard evolutionary track at $1.2\,M_\odot$. At that time, the luminosity is L_* and the effective temperature $T_{\rm eff}$. t^a is the age of the accreting star given by the model and t^s its value deduced from the HRD location; $\Delta t = t^s - t^a$.

star	L_* ($L_\odot$)	$T_{\rm eff}$ (K)	t^a (yr)	t^s (yr)	$\Delta t/t^s$
			$M_* = 0.9\,M_\odot$		
R1	4.42	4392	$4.04\ 10^5$	$4.2\ 10^5$	0.04
R2	0.57	4324	$4.01\ 10^6$	$5.3\ 10^6$	0.24
R3	1.60	4429	$1.25\ 10^6$	$1.37\ 10^6$	0.09
			$M_* = 1.2\,M_\odot$		
R1	2.59	4630	$1.15\ 10^6$	$1.17\ 10^6$	0.02
R2	1.27	5300	$12.97\ 10^6$	$15.32\ 10^6$	0.15
R3	1.80	5660	$17.65\ 10^6$	$18.24\ 10^6$	0.03

where t is the age of the star. If both stars are completely convective, they are located on the same Hayashi line and they thus have same mass provided their chemical composition is the same. Then, Eqs. (21) and (25) lead to

$$\frac{M^a(t^a)}{T_c^a(t^a)} = \frac{M^s}{T_c^s(t^s)} \,. \tag{26}$$

Since $M^a(t^a) = M^s$, we have

$$T_c^a(t^a) = T_c^s(t^s) \,. \tag{27}$$

From the previous paragraph, we know that

$$T_c^a(M^a(t^a)) > T_c^s(M^s) \,, \tag{28}$$

and, since the central temperature is a strictly increasing function of time (as well as the mass of our accreting star)

$$\frac{{\rm d}T_c}{{\rm d}t} > 0 \,, \tag{29}$$

it results, from relation (27) under the conditions imposed by Eqs. (28) and (29), that

$$t^a < t^s \,. \tag{30}$$

In other words, accretion delays the evolution of accreting stars; they appear younger than in the standard evolution. To illustrate this point we have estimated the time at which the accreting star reaches $0.9\,M_\odot$ and $1.2\,M_\odot$ (Table 1). Note however that the maximum age differences are rather modest ($\lesssim 20\%$).

5. Post accretion tracks

In this section we focus on evolution from the end of the accretion phase to the arrival on the zero age main sequence (ZAMS) at an age of about 3×10^7 yr (for $1.2\,M_\odot$).
Once accretion is finished, deuterium abundance falls immediately to its equilibrium value corresponding to a mass fraction

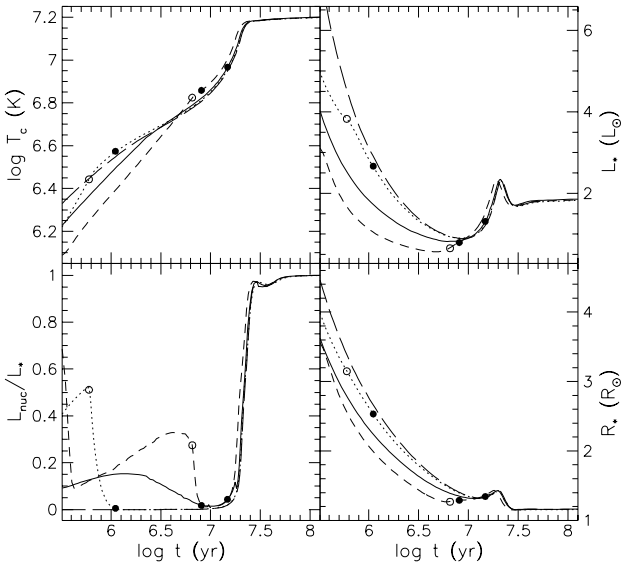

Fig. 14. Post accretion phase. This figure represents a panel of relevant variables from the end of accretion to the arrival on the MS. The solid, dotted and small-dashed curves refer to the accretion laws (R1), (R2) and (R3), respectively. The long dashed line is associated with a standard evolution of a $1.2\,M_\odot$ with the same chemical composition. Open circles indicate the time of the exponential decrease for the (R1) and (R2) prescription while empty circles mark the end of accretion for each star.

$X_D \sim 10^{-17}$. At the same time, the nuclear energy production vanishes and restores gravitation as the only energy source able to provide the luminosity. Their further evolution is very slow and the structural differences present at the end of the accretion phase are maintained. During this phase, contraction proceeds, the central temperature increases and ^{7}Li is depleted. When T_c reaches $\sim 1.3 \times 10^7$K, the ^{12}C(p,γ)^{13}N reaction ignites and its highly temperature sensitive energy production results in the development of a convective core. The central temperature rise is halted when most of the energy radiated away by the star is supplied by the nuclear sources (the contraction stops). As ^{12}C is depleted near the center and reaches its equilibrium abundance, the CNO cycle now provides the dominant source of energy and the star joins the main sequence (MS). Fig. 14 summarizes the evolution of key variables from the end of the accretion phase to their arrival on the MS.

6. Summary

Our study of accreting low-mass stars has revealed that deuterium burning is the main energetic support of the star. To follow its abundance evolution, it was necessary to couple the nucleosynthesis of this element with the equations of the stellar structure. The extreme temperature sensitivity of the deuterium destruction reaction rate produces a thermostatic effect that modifies the global structure. The more energy is provided to the star, either by increasing the accretion rate, the deuterium abundance or with the addition of ε_{acc}, the more it is converted to work against contraction. The reaction of the star prevents the

temperature and, in the same way, the nuclear energy production to climb drastically. It results from the thermostatic effect of deuterium burning. Consequently the star expands, its effective temperature being imposed by the great dependence of opacity on the temperature in the photosphere (along the Hayashi line), the emergent luminosity increases as well. Finally, once accretion ends, the star relaxes to its standard structure. On the main sequence, the star does not present any difference with respect to a non accreting model within similar properties.

The profile of accreted matter modifies the structural response of the star. When mass deposition is confined to the surface layers, less internal energy is given to the central regions and the star experiences a stronger contraction that yields to a higher central temperature. Moreover, this study has shown the small hydrostatic influence of mass accretion; this effect is much smaller than the effect of deuterium burning.

Comparison with standard PMS evolution indicates that the accretion process accelerates the evolution of the star. The central temperature of an accreting star is always larger than in a non accreting scheme. From its position in the HRD, it appears systematically younger. Especially during the earlier accretion phase, age estimate can be affected by up to a factor 2-3. These results as well as prediction concerning chemical abundances will be confronted to observations in Siess et al. (1997).

This study has revealed that the evolution of an accreting star results from two antagonistic effects, (i) the deuterium burning which tends to force the star to expand and (ii) the mass addition which reinforces the gravitational potential of the star and accelerates the contraction. Therefore, it is the combination of both $\dot{M}$and X_D that determines the further evolution of PMS accreting stars.

We will present, in a forthcoming paper, results of computations performed with high ($\dot{M} \gtrsim 10^{-6}\mathrm{M}_\odot\ \mathrm{yr}^{-1}$) accretion rates, in order to reproduce the birthline. These calculations will be compared with similar results obtained by Palla & Stahler (1990 and following papers).

Acknowledgements. We thank the referee, F. Palla, for his valuable and convenient comments and suggestions. The computations presented in this paper were performed at the "Centre de Calcul Intensif de l'Observatoire de Grenoble" and at "Informatique Mathématiques Appliquées Grenoble" on a IBM SP1 computer. These facilities are financed by the MESR, CNRS, and Région Rhône-Alpes.

Appendix A: species conservation

A.1. Mass fraction

Consider a species i whose mass fraction in the accreted matter and in the star at shell j are $X^a_{i,j}$ and $X^*_{i,j}$, respectively. The total mass of element i after accretion is given by $M^{*+a}_i = M^*_i + M^a_i$ and represent a summation over the n shells of the model:

$$M^{*+a}_i = \sum_{j=1}^{n} X^{*+a}_{i,j}\Delta m^{*+a}_j = \sum_{j=1}^{n} X^{*+a}_{i,j}(1+f_j)\,\Delta m^*_j$$
$$= M^*_i + M^a_i$$
$$= \sum_{j=1}^{n} X^*_{i,j}\Delta m^*_j + \sum_{j=1}^{n} f_j\, X^a_{i,j}\Delta m^*_j\ .$$

So, we have

$$\sum_{j=1}^{n} X^{*+a}_{i,j}(1+f_j)\,\Delta m^*_j = \sum_{j=1}^{n}(X^*_{i,j} + f_j\, X^a_{i,j})\Delta m^*_j\ ,$$

and finally we obtain

$$X^{*+a}_{i,j} = \frac{X^*_{i,j} + f_j\, X^a_{i,j}}{1 + f_j}\ .$$

A.2. Rescaled abundances

The new fractional mass $X^{*+a}_{i,k}$ derived alone refers to the old mesh point. However, modifications of the mass profile can result in changes in the mesh points. If k is the shell number such that $m_{j-1} \le m_k < m_j$ where subscript j refers to the old mesh points and k to the current ones, the interpolated composition at mass m_k is then

$$X^{*+a}_{i,k} = X^{*+a}_{i,j-1} + \left(\frac{\mathrm{d}X^{*+a}_{i,j}}{\mathrm{d}m}\right)_{j-1}(m_k - m_{j-1})\ .$$

References

Adams F.C., Emerson J.P., Fuller G.A., 1990, ApJ, 357, 606
Beckwith S.V.W., Sargent A.I., Chini R.S., Güsten, R., 1990, AJ, 99, 924
Bodenheimer P., Yorke H.W., Rozyczka M., Tohline J.E., 1990, ApJ, 355, 651
Braun N., Langer N., 1995, A&A, 297, 483
Cabrit S., Guilloteau S., Andre P., Bertout C., Montmerle T., Schuster K., 1996, A&A, 305, 527
Cassen P., Shu F., Terebey S., 1985, in Protostars & planets II, eds. D.C. Black and M.S. Matthews (Tucson: University of Arizona Press) p48
Caughlan G.R., Fowler W.A., 1988, Atomic Data Nucl. Data Tables 40, 283
Cox J.P., Giuli R.T., 1968, in Principles of stellar structure Gordon and Breach, Science Publishers
Forestini M., 1991, Ph. D.Thesis (Université Libre de Bruxelles, Belgium)
Forestini M., 1994, A&A, 285, 473
Hartmann L.W., Kenyon S.J., 1990, ApJ, 349, 190
Hayashi C. 1961, PASJ, 13, 450
Kenyon S.J., Hartmann L.W., 1990, ApJ, 349, 197
Kippenhahn R., Meyer-Hofmeister E., 1977, A&A, 54, 539
Larson R.B., 1969, MNRAS, 145, 271
Lin D.N.C, and. Pringle J.E, 1990, ApJ, 358, 515
Mercer-Smith J.A., Cameron A.G.W., Epstein R.I., 1984, ApJ, 279, 363
Mundt R., 1985, in protostars and planets II, eds D.C. Black and M.S. Matthews (Tucson: University of Arizona Press), pp 414
Palla F., Stahler S.W., 1990, ApJ, 360, L47
Palla F., Stahler S.W., 1991, ApJ, 375, 288 (PS)
Palla F., Stahler S.W., 1992, ApJ, 392, 667
Pophan R., Narayan R., Hartmann L., Kenyon S., 1993, ApJ, 415, L127
Regev O., Bertout C., 1995, MNRAS, 272, 71

Sargent A.I., Beckwith S.V.W., 1991, ApJ letter, 382, 31
Siess L., Bertout C., Forestini M., 1997, A&A, submitted
Siess L., Forestini M., 1996a, A&A, 308, 472 (SF)
Siess L., Forestini M., Dougados, C. 1996b, submitted
Shaviv G., Starrfield S., 1988, ApJ, 335, 383
Snell R.L., Loren R.B, Plambeck R.L., 1980, ApJ letter, 239, 17
Stringfellow G.S., 1989, Ph.D. Thesis. University of California at Santa Cruz.
Stahler S.W, Shu F.H., Taam R.E., 1980a, ApJ, 241, 637
Stahler S.W, Shu F.H., Taam R.E., 1980b, ApJ, 242, 226
Stahler S.W, 1988, ApJ, 332, 804
Terebey S., Shu F., Cassen P., 1984, ApJ, 286, 529
Winkler K.H., Newman M.J., 1980a, ApJ, 236, 101
Winkler K.H., Newman M.J., 1980b, ApJ, 238, 311
Yorke H.W., Bodenheimer P., Laughlin G., 1993, ApJ, 411, 651
Yorke H.W., Bodenheimer P., Laughlin G., 1995, ApJ, 443, 199

This article was processed by the author using Springer-Verlag LaTeX A&A style file *L-AA* version 3.